Atypical TRAV1-2$^-$ T cell receptor recognition of the antigen-presenting molecule MR1

Received for publication, July 20, 2020 Published, Papers in Press, August 14, 2020, DOI 10.1074/jbc.RA120.015292

Wael Awad[1,2], Erin W. Meermeier[3], Maria L. Sandoval-Romero[1], Jérôme Le Nours[1,2], Aneta H. Worley[4], Megan D. Null[5], Ligong Liu[6,7], James McCluskey[8], David P. Fairlie[6,7], David M. Lewinsohn[3,4,9], and Jamie Rossjohn[1,2,10,*]

From the [1]Infection and Immunity Program and Department of Biochemistry and Molecular Biology, Biomedicine Discovery Institute, Monash University, Clayton, Victoria, Australia, [2]ARC Centre of Excellence in Advanced Molecular Imaging, Monash University, Clayton, Victoria, Australia, [3]Department of Molecular Microbiology & Immunology, Oregon Health & Science University, Portland, Oregon, USA, [4]Veterans Affairs Portland Health Care Center, Portland, Oregon, USA, [5]Department of Pediatrics, Oregon Health & Science University, Portland, Oregon, USA, [6]Institute for Molecular Bioscience, University of Queensland, Brisbane, Queensland, Australia, [7]ARC Centre of Excellence in Advanced Molecular Imaging, University of Queensland, Brisbane, Queensland, Australia, [8]Department of Microbiology and Immunology, Peter Doherty Institute for Infection and Immunity, University of Melbourne, Melbourne, Australia, [9]Department of Pulmonary & Critical Care Medicine, Oregon Health & Science University, Portland, Oregon, USA, [10]Institute of Infection and Immunity, Cardiff University School of Medicine, Cardiff, Wales, United Kingdom

Edited by Peter Cresswell

MR1 presents vitamin B–related metabolites to mucosal associated invariant T (MAIT) cells, which are characterized, in part, by the TRAV1-2$^+$ $\alpha\beta$ T cell receptor (TCR). In addition, a more diverse TRAV1-2$^-$ MR1-restricted T cell repertoire exists that can possess altered specificity for MR1 antigens. However, the molecular basis of how such TRAV1-2$^-$ TCRs interact with MR1–antigen complexes remains unclear. Here, we describe how a TRAV12-2$^+$ TCR (termed D462-E4) recognizes an MR1–antigen complex. We report the crystal structures of the unliganded D462-E4 TCR and its complex with MR1 presenting the riboflavin-based antigen 5-OP-RU. Here, the TRBV29-1 β-chain of the D462-E4 TCR binds over the F′-pocket of MR1, whereby the complementarity-determining region (CDR) 3β loop surrounded and projected into the F′-pocket. Nevertheless, the CDR3β loop anchored proximal to the MR1 A′-pocket and mediated direct contact with the 5-OP-RU antigen. The D462-E4 TCR footprint on MR1 contrasted that of the TRAV1-2$^+$ and TRAV36$^+$ TCRs' docking topologies on MR1. Accordingly, diverse MR1-restricted T cell repertoire reveals differential docking modalities on MR1, thus providing greater scope for differing antigen specificities.

MR1 is a monomorphic antigen (Ag)–presenting molecule that captures and presents a broad range of small organic compounds. Several MR1 antigens have been described, including folate (vitamin B9)–derived antigens, such as 6-formylpterin (6-FP) and its synthetic derivative acetyl-6-FP (Ac-6-FP) (1–3). Likewise, MR1 presents microbial metabolites of riboflavin precursors, which are derived from a wide range of riboflavin-producing microbes (1, 2, 4–6). These riboflavin derivatives include the ribityl-lumazines 7-hydoxy-6-methyl-8-D-ribityllumazine (RL-6-Me-7-OH) and 6,7-dimethyl-8-D-ribityllumazine (RL-6,7-diMe), and some extremely potent uracil-based antigens such as 5-(2-oxopropylideneamino)-6-D-ribitylaminouracil (5-OP-RU). Furthermore, MR1 was recently found to display a diverse panel of small chemical scaffolds such as drugs, druglike, and drug metabolites, including analogues of the anti-inflammatory drugs aspirin and diclofenac (7). Interestingly, a recent report suggested that MR1 presents nonmicrobial tumor cell–derived metabolites, although the ligand identity is yet to be identified (8). Accordingly, MR1 exhibits sufficient plasticity to present a chemically diverse range of small hydrophobic organic molecules. These ligands are sequestered within the aromatic cradle residues of the MR1 A′-pocket, whereas no physiological ligands have been described to bind within the neighboring F′-pocket of MR1. Notably, many MR1 antigens form a Schiff base covalent bond with Lys-43 within the A′-pocket of MR1, an interaction that plays a prominent role in stabilizing the ligands inside the pocket and allowing MR1 to egress to the cell surface (1, 2, 6, 9, 10).

MR1 presents such antigens to defined populations of $\alpha\beta$ and $\gamma\delta$ T cells, with the majority of MR1-restricted T cells being mucosal associated invariant T (MAIT) cells (11–17). MAIT cells are an abundant innate-like T cell population in mammals and are mainly localized at the mucosa, liver, peripheral blood, and lung (12, 18–25). Human MAIT cells express a semi-invariant T cell receptor (TCR), comprised of an α-chain of an invariant *TRAV1-2* gene frequently recombined with *TRAJ33*, *TRAJ12*, or *TRAJ20* segments, paired with a biased set of *TRBV* genes including *TRBV6* and *TRBV20* (12). Much of the diversity in the classical MAIT TRAV1-2$^+$ TCR repertoire is found within the complementarity determining region (CDR) 3β loop, which can fine-tune MR1–antigen recognition (3, 14, 26, 27). Riboflavin-related antigens can activate MAIT cells with varying degrees of potency, with 5-OP-RU representing the most potent MAIT agonist described to date. In contrast, folate-based ligands do not activate MAIT cells in general (1, 2). Structural investigations show that these TRAV1-2$^+$ MAIT TCRs dock similarly atop the A′-pocket of MR1, where the ribityl 2′-OH group of the stimulating ligands forms an

* For correspondence: Jamie Rossjohn, Jamie.rossjohn@monash.edu.

"interaction triad" with the MR1–Tyr-152 and the evolutionary conserved Tyr-95α from the CDR3α loop. Disruption of this interaction triad has been linked to a loss of potency for known MAIT cell antigens (2, 3, 6, 28, 29).

A diverse population of MR1-restricted αβ T cells that do not utilize the conventional TRAV1-2 chain, called atypical TRAV1-2$^-$ MR1-resticted T cells, have been identified through MR1-Ag tetramer staining of human peripheral blood mononuclear cells (14, 16, 30, 31). Moreover, other identified TRAV1-2$^-$ MR1-restricted T cells exhibit differing reactivities to folate, riboflavin, MR1 autoreactivity, or reactivities to unknown ligands that appear to be a function of the αβTCR gene usage (5, 15, 16, 19, 30–33). Recent studies identified TRAV36$^+$ MR1–5-OP-RU reactive T cell clones that have been detected in various unrelated human donors, suggesting a public TRAV1-2$^-$ MR1-reactive TCR repertoire (16, 30). The crystal structure of one of these TCRs, MAV36 (TRAV36/TRAJ34-TRBV28), complexed with MR1–5-OP-RU was determined and showed a more central docking of MAV36 TCR on the MR1 cleft than for TRAV1-2$^+$ MAIT TCRs (30). Other TRAV1-2$^-$ MR1-restricted T cell clones have been described (31) and one of these clones (D462-E4) carries the TRAV12-2/TRAJ39 paired with TRBV29-1/TRBJ01-05 gene. Interestingly, the D462-E4 T cell clone showed a distinct pattern of ligand and microbial recognition in detecting infection by riboflavin-producing microbes and certain riboflavin-auxotroph *Streptococcus pyogenes* microbes in a TCR-dependent manner (31). Accordingly, this TCR could recognize specific riboflavin-based, and unidentified non–riboflavin based, ligands (5, 31). How this particular TCR interacted with MR1 remained unknown.

To expand our molecular understanding of how human TRAV1-2$^-$ TCRs recognize MR1, we determined the crystal structure of unliganded D462-E4 TCR and its complex with the MR1–5-OP-RU adduct. Our data reveal that the TRAV12-2–TRBV29-1 TCR adopts a distinctly different molecular footprint atop MR1 compared with TRAV1-2$^+$ MAIT TCR-MR1-Ag and MAV36$^+$ TCR-MR1-Ag ternary complexes. Accordingly, we provide a new understanding of how diverse αβTCR usage manifests in differing MR1 docking geometries.

Results

Characteristics of MR1-restricted TRAV12-2/TRBV29-1 T cell clone

Previously, we identified T cell clones that bound to the MR1–5-OP-RU tetramer, yet expressed atypical TRAV1-2$^-$ MR1-restricted TCRs; one of these T cell clones is referred to as D462-E4 (31). Both D462-E4 and MAIT TRAV1-2$^+$ T cell clones expressed CD8α and stained with the MR1–5-OP-RU tetramer to similar levels of intensity, but not to the MR1–6-FP tetramer (Fig. 1*a*). TCR sequencing of the D462-E4 T cell clone showed that the TCR α-chains and TCR β-chains were composed of TRAV12-2/TRAJ39-01 and the TRBV29-1/TRBJ01-05 gene segments, respectively (Table 1). The D462-E4 TCR does not contain the critical Tyr-95α residue from the CDR3α loop, which interacts with 5-OP-RU in the TRAV1-2$^+$ TCR-MR1–5-OP-RU ternary structures (2).

To investigate the MR1-restricted function and activation potency of the D462-E4 T cell clone, we used a plate-bound tetramer ELISPOT (tetraSPOT) assay to measure the IFN-γ release upon T cell activation. Here, both MR1–5-OP-RU and MR1–6-FP tetramers were immobilized onto the plate and IFN-γ production of both TRAV1-2$^-$ (D462-E4) and MAIT TRAV1-2$^+$ (D426-G11) T cell clones was quantified against titrated tetramer concentrations (Fig. 1*b*). Both TRAV1-2$^-$ and TRAV1-2$^+$ T cell clones responded to MR1–5-OP-RU (not to MR1–6-FP) and showed similar maximal efficacy (IFN-γ release) (Fig. 1*b*). The antigen concentration of half-maximal response (EC_{50}) of MR1–5-OP-RU for the atypical MR1-restricted D462-E4 T cell clone was 0.11 nM, whereas the EC_{50} for the control MAIT cell clone was 0.002 nM. The response to MR1–5-OP-RU by D462-E4 was inhibited by an MR1-blocking antibody, confirming MR1 restricted T cell function (Fig. 1*c*). Collectively, the D462-E4 TRAV1-2$^-$ TCR displayed similar maximal efficacy, but lower TCR avidity and potency of 5-OP-RU antigen dose, compared with the TRAV1-2$^+$ MAIT TCRs.

D462-E4 TCR exhibits moderate affinity for MR1–5-OP-RU

To establish how the D462-E4 TRAV1-2$^-$ TCR binds to the MR1 molecule, we expressed the extracellular domains of the D462-E4 TCR as inclusion bodies in *Escherichia coli*, and the D462-E4 TCR was refolded into its native conformation and purified as summarized under "Experimental procedures." Next, we conducted surface plasmon resonance (SPR) experiments to compare the specificities and binding affinities of both of A-F7 (TRAV1-2–TRBV6-1) and D462-E4 (TRAV12-2–TRBV29-1) TCRs against MR1 presenting the 5-OP-RU, 6-FP, or Ac-6-FP ligands (Fig. 2). As previously reported, A-F7 TCR recognized MR1–5-OP-RU with high affinity (K_D = 2.2 ± 0.4 μM) and showed weak binding to MR1–Ac-6-FP and MR1–6-FP proteins (K_D = 88.2 ± 20 and 101.2 ± 30 μM, respectively).

Consistent with the activation data (Fig. 1), whereas the D462-E4 and AF-7 TCRs exhibited similar affinity against MR1–Ac-6-FP and MR1–6-FP (~80–100 μM), the affinity of the D462-E4 TCR for MR1–5-OP-RU was a 7-fold lower affinity than that of the A-F7 TCR (K_D = 16.3 ± 1.1 μM). Collectively, both A-F7 and D462-E4 TCRs were riboflavin-based ligand reactive TCRs, yet they exhibited differing affinities toward MR1–5-OP-RU.

Overview of the D462-E4 TCR-MR1–5-OP-RU ternary complex

Next, we determined the crystal structure of the D462-E4 TCR-MR1–5-OP-RU ternary complex to 2.9 Å resolution (Table 2 and Figs. 3 and 4). The D462-E4 TCR docked orthogonally atop the MR1 antigen binding cleft (Fig. 3, *d* and *e*). The buried surface area (BSA) at the interface between D462-E4 TCR and MR1 was ~1070 Å^2, a value that falls within the range of BSA values of TRAV1-2$^+$ MAIT TCR-MR1-Ag complexes (1050–1200 Å^2) (6, 29). Although the α- and β-chains of MR1-restricted TCRs contributed almost equally to the BSA of the interfaces of most TCR-MR1-Ag complexes, the α- and β-chains of the D462-E4 TCR contributed to ~39 and 61%, respectively, with this difference being attributed to a differing MR1 docking modality of the D462-E4 TCR (Fig. 3).

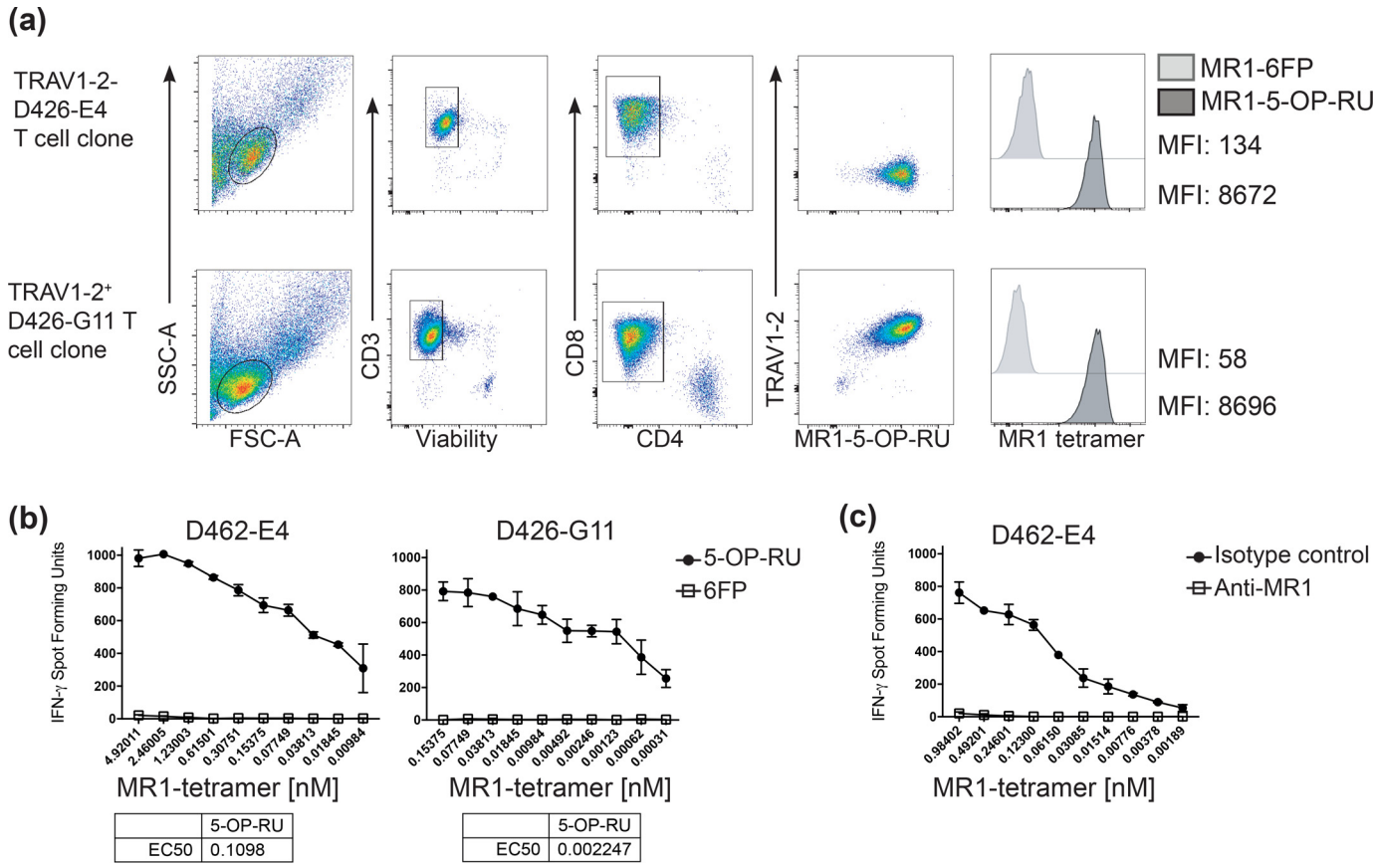

Figure 1. An atypical TRAV12-2$^+$ T cell clone is activated by MR1–5-OP-RU. *a*, staining of T cell lineage markers, TRAV1-2 TCR, with MR1 tetramers loaded with either 6-FP or 5-OP-RU on two T cell clones: D462-E4 (*top*) and D426-G11 (*bottom*). Geometric mean fluorescence intensity (*MFI*) of the MR1-tetramer staining is shown in the inset in the overlaid histograms. *b*, TCR $\alpha\beta$ gene names and CDR3 amino acid sequences of the D462-E4 T cell clone. *c*, T cell clone IFN-γ responses to MR1-6FP (*open squares*) or MR1-5-OP-RU tetramer (*black circles*) dilutions at concentrations listed on the *x* axis. MR1 blocking antibody (*open circles*) or its isotype control (*black squares*) was also added to MR1-5-OP-RU Tetraspot wells as indicated. IFN-γ response is quantified by spot forming units of ELISPOT assay. The EC_{50} for each clone's response to MR1-5-OP-RU is listed under the graph. *Error bars* represent the mean and S.D. from technical replicates.

Table 1
TCR sequences

	TCRα					TCRβ				
Tcr	**Trav**	**Traj**	**CDR1α**	**CDR2α**	**CDR3α**	**Trbv**	**Trbj**	**CDR1β**	**CDR2β**	**CDR3β**
D426-E4	TRAV12	TRAJ39	^{28}DRGSQSF^{34}	^{51}IYSNGD^{56}	^{90}CAVRDAGNMLTF^{101}	TRBV29-1	TRBJ1-5	^{28}SQVTM^{32}	^{50}ANQGSEAT^{57}	^{94}CSVGGDSLIGNQPQHF^{109}
A-F7	TRAV1-2	TRAJ33	^{26}TSGFNG^{31}	^{49}NVLDGL^{53}	^{88}CAVKDSNYQLI^{98}	TRBV6-1	TRBJ2-2	^{27}MNHNS^{31}	^{49}SASEGT^{54}	^{92}ASSVWTGEGSGELF^{105}
MAV36	TRAV36	TRAJ34	^{27}VTNFRS^{32}	^{49}LTSSGIE^{55}	^{89}CAAYNSDKLIF^{99}	TRBV28	TRBJ2-5	^{27}MDHEN^{31}	^{49}SYDVKM^{54}	^{91}CASSPSGYQETQYF^{104}

The electron density of 5-OP-RU and residues at the D462-E4 TCR/MR1 molecular interface was unambiguous. Here, the 5-OP-RU ligand in the D462-E4 TCR-MR1–5-OP-RU complex was typically sequestered within the MR1 A′-pocket and formed a Schiff base covalent bond with MR1–Lys-43 (Fig. 4*c*). The interactions made with the ligand uracil ring, as well as the 2′- and 3′-OH groups of the ribityl moiety of 5-OP-RU were conserved compared with the TRAV1-2$^+$ TCR-MR1–5-OP-RU complexes. Nevertheless, the 4′-OH and 5′-OH groups of the ribityl chain in the D462-E4 TCR-MR1–5-OP-RU structure exhibited two alternate conformations within the pocket, each having 50% occupancy (Fig. 4, *c*, *d*, and *e*). This resulted in greater surface exposure and accessibility of the ribityl moiety, where one conformation was oriented toward the F′ pocket of MR1 and contacted the CDR3β loop. Further, structural modifications within the MR1 antigen binding cleft were observed upon D462-E4 TCR binding compared with the TRAV1-2$^+$ TCR-MR1 complexes (Fig. 4). Here, part of the MR1 α2-helix (Trp-143 to Asn-155) was slightly displaced (root mean square deviation (rmsd), 0.53 Å) (Fig. 4*b*), as a result of its interactions with the CDR3β loop compared with the TRAV1-2$^+$ TCR-MR1 complexes (described below). Collectively, this reflects the adaptability of the MR1 Ag-binding cleft, and its sequestered ligand, upon ligation with the MR1-reactive TCRs.

Atypical TRAV1-2$^-$ TCR-MR1 and TRAV1-2$^+$ MAIT TCR-MR1 contacts are disparate

All MR1-restricted $\alpha\beta$ TCRs docked atop the MR1 antigen binding cleft whereby the TCRs α- and β-chains resided over the α2- and α1-helix of MR1, respectively (29). The D462-E4 TCR also docked similarly atop the MR1 antigen binding cleft,

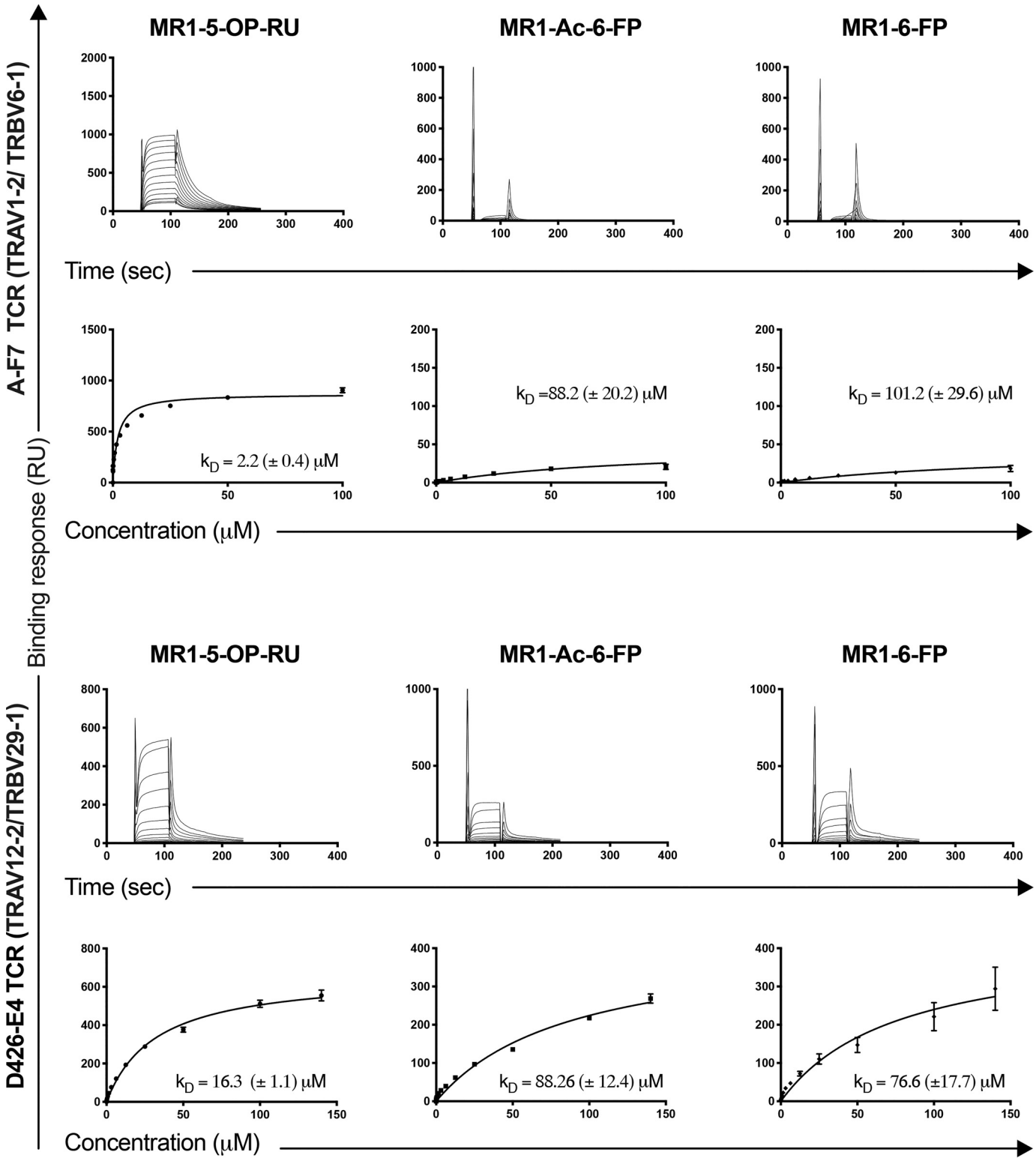

Figure 2. Steady-state affinity measurements of MR1-restricted TCRs. The affinity of TCR-MR1-Ag interactions were determined using SPR, by measuring the binding of various concentrations of soluble TRAV1-2$^+$ A-F7 TCR (100–0.024 μM) and TRAV1-2$^-$ D426-E4 TCR (140–0.024 μM) against human MR1 refolded with 5-OP-RU, Ac-6-FP, and 6-FP. SPR runs were conducted as duplicate in three independent experiments using different batches of proteins. The SPR sensograms, equilibrium curves, and steady state K_D values (μM) were prepared in GraphPad Prism 7.

but more toward the MR1 F′-pocket (Fig. 3*d*), whereas the TRAV1-2$^+$ MAIT TCRs sat orthogonally to the A′-pocket of MR1 (Fig. 3, *a–c*) (29). Here, the center of gravity of the D462-E4 TCR β-chain was displaced ~5 Å toward the MR1 F′-pocket compared with the β-chain of TRAV1-2$^+$ MAIT TCR-MR1 complexes. Nevertheless, the TRAV12-2 α-chain adopted a similar position to the TRAV1-2 chain of MAIT TCRs (Fig. 4, *a* and *b*). Further, the D462-E4 TCR was rotated ~11° compared

Table 2
Data collection and refinement statistics

	D426-E4 TCR-MR1-5-OP-RU	D426-E4 TCR
Resolution range (Å)	44.8–2.9 (3.00–2.90)	40.74–2.68 (2.78–2.68)
Space group	P 21 21 21	P 43 2 2
Unit cell a, b, c (Å)	101.877 113.433 209.606	115.222 115.222 183.992
α, β, γ (°)	90 90 90	90 90 90
Total reflections	109,131 (10724)	70,760 (6885)
Unique reflections	54,572 (5362)	35,384 (3444)
Multiplicity	2.0 (2.0)	2.0 (2.0)
Completeness (%)	99.92 (100.00)	99.56 (99.28)
Mean I/σ(I)	10.11 (2.37)	26.62 (4.91)
Wilson B-factor	43.56	45.04
R_{merge}	0.07439 (0.3277)	0.02418 (0.1512)
R_{pim}	0.07439 (0.3277)	0.02418 (0.1512)
CC1/2	0.99 (0.513)	0.999 (0.799)
R_{work}	0.1885 (0.2765)	0.1945 (0.2606)
R_{free}	0.2335 (0.3326)	0.2237 (0.2947)
Nonhydrogen atoms	12,963	6923
Macromolecules	12,495	6765
Ligands	137	6
Solvent	331	152
Protein residues	1578	879
RMS (bonds) (Å)	0.002	0.002
RMS (angles) (°)	0.53	0.47
Ramachandran favored (%)	98.25	96.31
Ramachandran allowed (%)	1.75	3.69
Ramachandran outliers (%)	0.00	0.00
Average B-factor	43.59	49.60
Macromolecules	43.92	49.75
Ligands	36.47	67.24
Solvent	34.21	42.46

with TRAV1-2$^+$ MAIT TCRs, placing the β-chain closer to MR1, thereby allowing the TCR β-chain of D462-E4 TCR to participate in the recognition of MR1. Consequently, the D462-E4 TCR adopted markedly different footprints on MR1 compared with TRAV1-2$^+$ MAIT TCRs (Fig. 3, *c* and *f*).

In a comparison with the previously determined structure of the atypical MAV36-TCR-MR1–5-OP-RU complex (30), both MAV36 and D462-E4 TCRs located closer to the F′-pocket of MR1 (Fig. 3, *d* and *g*), whereas the MAV36 TCR docked 65° across the antigen binding cleft, making extensive interactions with the α1-helix of MR1 compared with the D462-E4 TCR (Fig. 3*h* and *i*). Accordingly, disparate docking modes underpin MR1–5-OP-RU recognition by TRAV1-2$^+$, MAV36, and D462-E4 TCRs.

Role of TCR TRAV12-2 α-chain in MR1 recognition

The D462-E4 TCR was characterized by TRAV12-2-TRAJ39-01 gene usage. Notably, the CDR1α, CDR2α and CDR3α loops of D462-E4 TCR docked above the MR1 A′-pocket, akin to the positions of the relevant loops of TRAV1-2$^+$ TCRs (Fig. 4*b*). Here, the CDR3α loop of D462-E4 contributed to ~16% BSA upon complexation with MR1 through forming hydrophilic and hydrophobic interactions with residues from the MR1 α1- and α2-helices (Fig. 5, *a* and *b*). Namely, Arg-93α flanked the MR1 α2-helix interacting with MR1–His-148 and –Tyr-152, whereas Ala-95α, Gly-96α, and Met-98α residues formed a network of interactions with the Arg-61, Tyr-62, and Leu-65 residues of the MR1 α1-helix (Table 3). Interestingly, this CDR3α loop did not show any direct or water-mediated interactions with 5-OP-RU. Indeed, the Asn-97α from the CDR3α loop, analogous to Tyr-95α in TRAV1-2$^+$ MAIT TCRs, was >6 Å away from 5-OP-RU.

The CDR1α, CDR2α loops and the Vα framework region sat close to the α2-helix and contributed only 6%, 10 and 7% to the complex BSA, respectively. Here, Gln32α of CDR1α formed hydrogen bonds with MR1-Asn155 and Glu160. While Tyr52α from the CDR2α loop extensively interacted with MR1-His148, Tyr152 and Asn155 (Fig. 5*c* and Table 3). Altogether, the TRAV12-2 TCR α-chain interactions was distinct from that of the TRAV1-2$^+$ TCR footprint on MR1.

Role of TRBV29-1 β-chain and its CDR3β loop in MR1 recognition

The TRBV29-1 β-chain contributed almost two thirds of the interface between D462-E4 TCR and MR1 (61% BSA). The Vβ framework region, CDR1β, and CDR2β extended above the α1-helix of MR1 and contributed 7%, 10 and 7% BSA, respectively, to the binding interface. The Vβ framework and the CDR1β loop bound MR1 mainly by hydrophobic interactions, whereas Asn-51β from the CDR2β loop H-bonded to MR1–Gln-64 (Table 3 and Fig. 5*d*).

Surprisingly, the CDR3β loop wedged between the helical jaws of the MR1 cleft, surrounding the F′-pocket, although proximal to the bound antigen in A′-pocket (Fig. 5, *e* and *f*). Notably, the CDR3β loop was the principal contributor to the D462-E4 TCR-MR1 interface, providing ~37% of the BSA and thus played a prominent role in the interaction and recognition of D462-E4 TCR by MR1. Moreover, the CDR1β loop played an important role in consolidating the CDR3β loop in a fixed configuration atop the F′-pocket of MR1 by forming H-bonds between Met-32β and Thr-31β from the CDR1β, and the Gly-97β and Asp-99β residues from the CDR3β, respectively.

Here, the ^{99}Asp-Ser-Leu-Ile-Gly-Asn^{104} segment had a dominant role in mediating CDR3β contacts with MR1 (Table 3 and Fig. 5*f*). The backbone of this peptide folded upon itself to produce a structural "hairpin turn" motif by forming three intramolecular H-bonds (Fig. 5*f*). This hairpin turn of CDR3β capped the F′-pocket and extensively interacted with various residues of MR1 α1- and α2-helices. Interestingly, the CDR3β Asp-99β and Asn-104β residues occupied the space between the A′- and F′-pockets, and their side chains were oriented toward the bound antigen in the A′-pocket. Asp-99β and Ser-100β formed various hydrophobic contacts with the Trp-69, Met-72, Val-75 and Glu-76 of MR1 α1-helix. In addition, the backbone carbonyl of Leu-101β formed H-bonds with the side chains of MR1–Arg-79 and –Trp-143 of α1- and α2-helices, respectively. On the other side of the hairpin turn, Ile-102β, Gly-103β, and Asn-104β residues extensively interacted with MR1–Ala-142, –Trp-143, –Asn-146, and –Glu-149 residues from the MR1 α2-helix (Table 3 and Fig. 5*f*). Accordingly, the CDR3β loop play a prominent role in the interaction and recognition of the D462-E4 TCR by the MR1 molecule.

Divergent recognition of riboflavin derivatives by MR1-restricted TCRs

The D462-E4 TRAV1-2$^-$ TCR presented Asn-97α in an equivalent position to the Tyr-95α of TRAV1-2$^+$ TCRs. However, the entire CDR3α loop of D462-E4 TCR and its Asn-97α were positioned >6 Å from 5-OP-RU, with no direct or water-

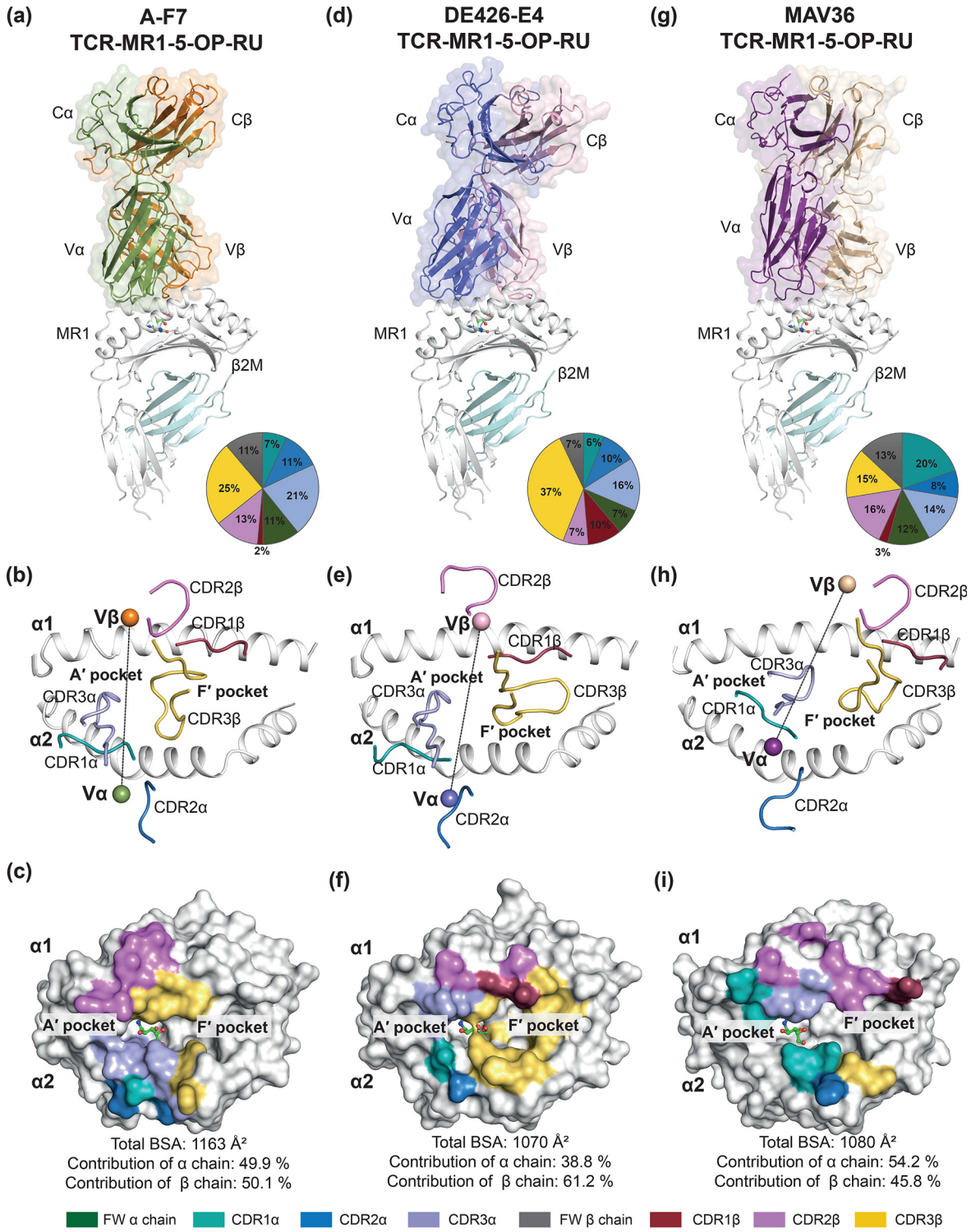

Figure 3. Structural comparison of ternary complexes of TRAV1-2$^+$ and TRAV1-2$^-$ TCRs with MR1-5-OP-RU. Crystal structures of ternary complexes. *a–c*, A-F7 (TRAV1-2/TRBV6-1) TCR-MR1-5-OP-RU (PDB ID: 4NQC). *d–f*, D426-E4 (TRAV12-2/TRBV29-1) TCR-MR1-5-OP-RU. *g–i*, MAV36 (TRAV36/TRBV28) TCR-MR1-5-OP-RU (PDB ID: 5D7L). *a*, *d*, and *g*, *top panels*, depict ribbon diagrams of the ternary complexes and pie charts representing the contribution of each TCR segment toward the MR1-5-OP-RU complex. The MR1 and β2-microglobulin molecules are colored *white* and *pale cyan*, respectively, and 5-OP-RU is presented as *green sticks*. A-F7 TCRα, *olive*; A-F7 TCRβ, *orange*; D426-E4 TCRα, *blue*; D426-E4 TCRβ, *light-pink*; MAV36 TCRα, *violet-purple*; MAV36 TCRβ, *light brown*. *b*, *e*, and *h*, *middle panels*, show the TCRs and their CDR loops docking into MR1. The center of mass of the respective TRAV and TRBV variable domains are shown as a *sphere* colored consistent with chain colors in the *upper panels*. The CDR loops are colored as follows: CDR1α, *teal*; CDR2α, *sky-blue*; CDR3α, *light-blue*; frameworks of α-chain, *dark-green*; CDR1β, *maroon*; CD2β, *violet*; CDR3β, *yellow-orange*; frameworks of β-chain, *dark-gray*. *c*, *f*, and *i*, lower panels, illustrate the TCR footprints on the molecular surface of MR1-5-OP-RU. The atomic footprint is colored according to the TCR segment making contact.

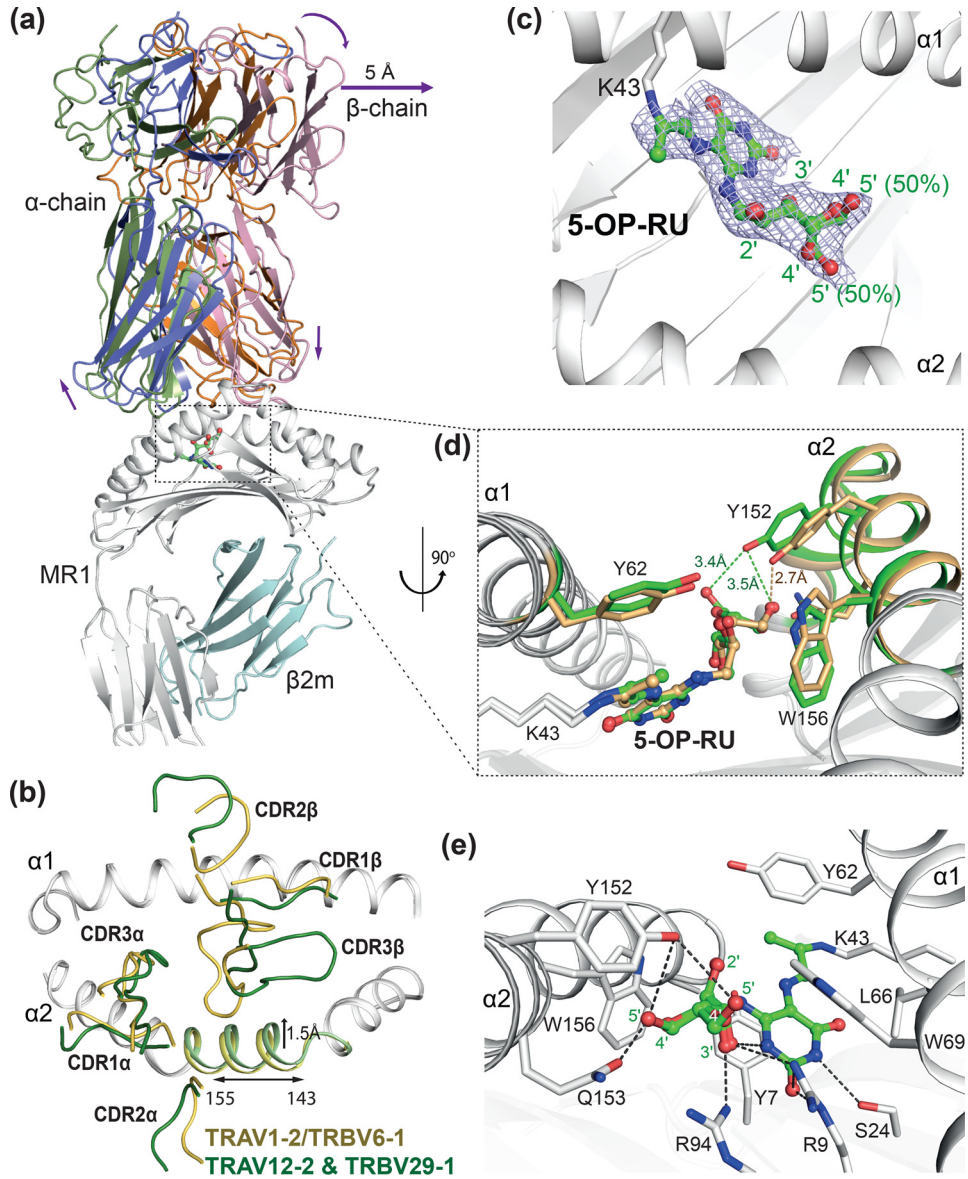

Figure 4. MR1 conformational changes upon interactions with D426-E4 TCR. *a*, comparison of TRAV1-2$^-$ D426-E4 ternary complex relative to the TRAV1-2$^+$ TCR docking positions. *Arrows* illustrate TCR rotation around the center of mass of the MR1, as well as displacement of *β*-chain along the MR1 binding cleft. The colors of the TCR chains are consistent with Fig. 3*a*. *b*, superposition of the CDR loops of A-F7 (*yellow*) and D426-E4 (*green*) TCRs sitting atop MR1. *c*, working ($2F_o - F_c$) map of 5-OP-RU inside MR1 pocket, showing two alternate conformations of the antigen. *d*, comparison of the MR1 antigen binding pocket and the position of Tyr-152 in both of A-F7 (*yellow*) and D426-E4 (*green*) ternary structures. *e*, interactions of 5-OP-RU and the residues of MR1 A′ portal in the D426-E4 TCR-MR1-5-OP-RU structure.

based contacts with ligand observed. Nevertheless, the side chain of MR1–Tyr-152 was H-bonded to the Asn-97*α*, as well as to the 5′-OH of both 5-OP-RU conformations (Fig. 6*a*). Asp-99*β* from the CDR3*β* loop oriented toward the A′-pocket of MR1 antigen binding cleft, forming a H-bond (2.9 Å) with the 5′-OH of one ribityl conformation (Fig. 6*a*).

The usage of the TRAV1-2 gene in MR1-restricted TCRs facilitates a consistent docking mode atop the MR1. This docking mode maintains the evolutionary conserved Tyr-95*α* from the CDR3*α* loop in a conserved location, so that it protrudes deeply into the A′-pocket of the MR1-Ag-binding cleft. This enabled H-bonding between Tyr-95α^{OH} and the 2′-OH of the ribityl moiety of the antigen, as well as MR1–Tyr-152 (Fig. 6*b*) (2, 3, 28). Indeed, Tyr-95*α*, Tyr-152 and 5-OP-RU formed an interaction triad that has been shown to play a prominent role in TRAV1-2$^+$ TCR recognition of MR1-presenting riboflavin derivatives (6). The structure of the MAV36 TCR-MR1–5-OP-RU complex showed that Asn-29*α* from the CDR1*α* loop was vital for recognition of 5-OP-RU, by forming a direct H-bond with the 2′-OH of the ribityl moiety (Fig. 6*c*) (30). Notably, the CDR3*α* Tyr-95*α* of TRAV1-2$^+$ TCRs and the CDR1*α* Asn-29*α* of MAV36 TCR were closely aligned in a position that enabled their side chains to interact with the 2′-OH of 5-OP-RU in a convergent recognition mechanism of the ligand. In contrast, Asp-99*β* from CDR3*β* loop of D462-E4 TCR interacted with the terminal 5′-OH group of 5-OP-RU. This reveals differential recognition of riboflavin-based metabolites by diverse MR1-restricted TCRs.

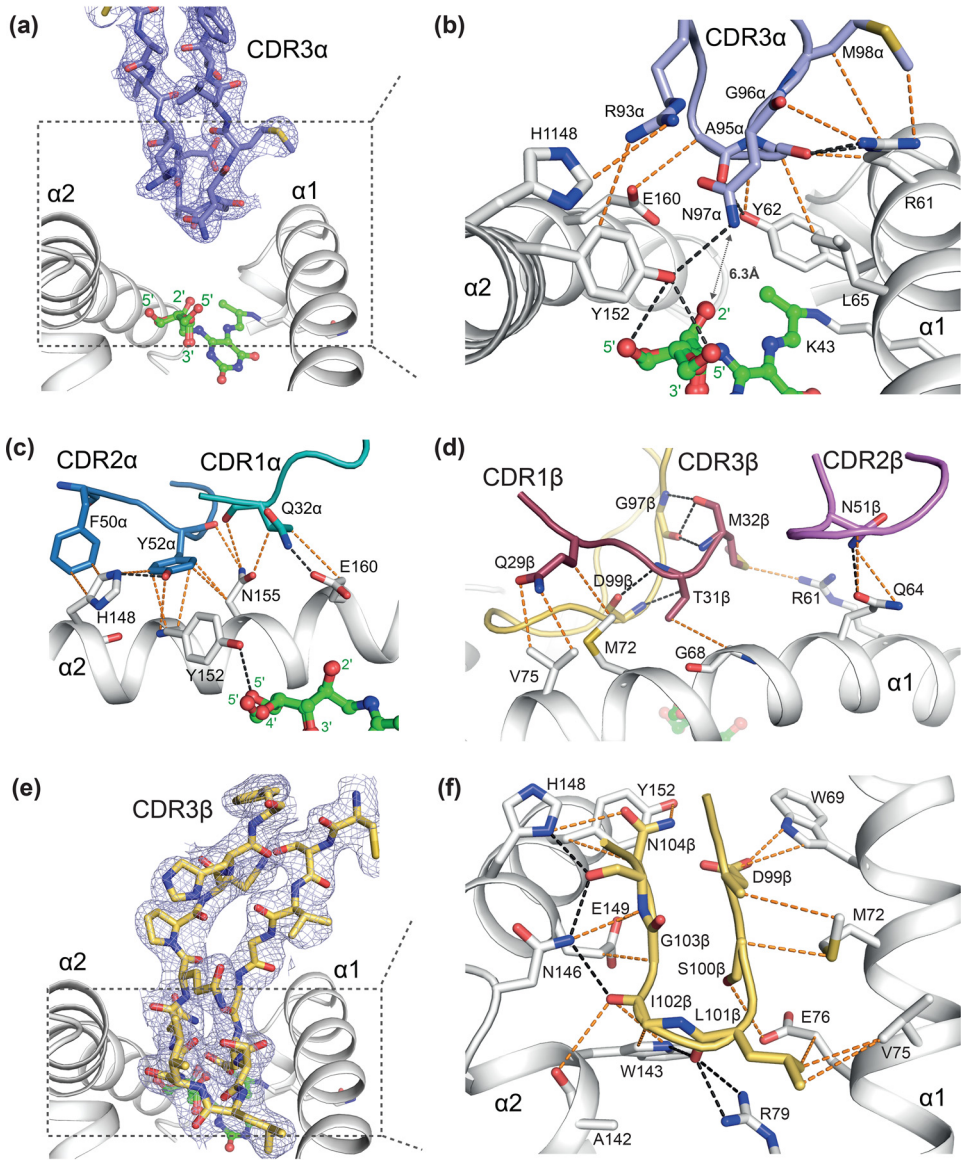

Figure 5. Molecular contacts of the D426-E4 TCR-MR1 complex. *a–f*, interactions between MR1 and (*a* and *b*) the CDR3α, (*c*) CDR1α and CDR2α, (*d*) CDR1β and CDR2β, and (*e* and *f*) CDR3β. The working ($2F_o - F_c$) map of CDR3α and CDR3β is shown in *panels a* and *e*, respectively. The colors of all loops are consistent with Fig. 3. The interacting residues are represented as *sticks*. Hydrogen bonds, and van der Waals interactions are represented by *black*, *orange dashes*, respectively. See also Table 3.

D462-E4 TCR lock and key recognition of the MR1–5-OP-RU molecule

To investigate the TCR conformational changes upon D462-E4 TCR recognition of MR1–5-OP-RU, we determined the crystal structure of the D462-E4 TCR in its unliganded state (Table 2 and Fig. 7*a*) and compared it to the structure of the D462-E4 TCR-MR1–5-OP-RU ternary complex. There was little displacement (rmsd, 0.94 Å) of the variable domain of the α-chain (Vα) and all CDRα loops upon binding to MR1 molecule, but with minimal changes to their side chain locations (Fig. 7*b*). Interestingly, with the exception for CDR3β, no appreciable movement or changes within the CDRβ loops were observed after MR1 engagement, suggesting that little conformational adjustments of the CDRβ loops were required for recognition of MR1 (Fig. 7, *c* and *d*). Indeed, the tip of the CDR3β loop slightly moved (rmsd 0.3 Å) to made favorable contacts with the F′-pocket of MR1. Collectively, the relatively rigid D462-E4 TCR recognized MR1 molecule by a lock and key mechanism.

Discussion

MR1 molecules present metabolite-related antigens to diverse populations of T cells, which are biased toward the usage of the TRAV1-2 gene (TRAV1-2$^+$) frequently paired with TRBV6 and 20. We and others have previously described diverse populations of TRAV1-2$^-$ MR1-restricted T cells in humans that use a broad range of TRAV, TRAJ, TRBV, and TRBJ genes including TRAV19$^+$, TRAV36$^+$, and TRAV12-2$^+$ subsets among others (8, 16, 26, 30, 31). These TRAV1-2$^-$ TCRs can exhibit altered specificity toward microbial and/or

Table 3
Contacts of D426-E4 TCR with MR1-5-OP-RU

Atomic contacts determined using the *CONTACT* program of the CCP4i package with cutoff of 4 Å. Hydrogen bond interactions are defined as contact distances of 3.5 Å or less. Van der Waals (VDW) interactions are defined as non-hydrogen bond contact distances of less than 4 Å. Salt bridge interactions are defined as contact distances of 4.5 Å or less.

TCR gene	TCR residue	MR1	Bond type
CDR1α	Gln-32	Glu160	H-bond
	Gln-32	Asn155 & GLu160	VDW
CDR2α	Tyr52	His148	H-bond
	Tyr52	His148, Leu151, Tyr152 & Asn155	VDW
	Phe50	His148	VDW
CDR3α	Arg93	His148 & Y152	VDW
	Ala95	Tyr62	H-bond
	Ala95	Glu160, Tyr62	VDW
	Gly96	Arg61	H-bond
	Gly96	Leu65 & Arg61	VDW
	Asn97	Tyr152	H-bond
	Asn97	Arg61 & Tyr152	VDW
	Met98	Arg61	VDW
α Framework	Phe35	His148	VDW
	Lys68	Asn155	VDW
CDR1β	Gln29	Met72 & Val75	VDW
	Thr31	Gly68	VDW
	Met32	Arg61	VDW
CDR2β	Asn51	Gln64	H-bond
	Asn51	Gln64	VDW
CDR3β	Asp99	Trp69 & Met72	VDW
	Leu101	Arg79 & Trp143	H-bond
	Leu101	Val75, Arg79 & Trp143	VDW
	Ile102	Asn146	H-bond
	Ile102	Ala142, Trp143, Asn146	VDW
	Gly103	Trp143 & Glu149	VDW
	Asn104	Asn146, His148, Glu149 & Tyr152	VDW
	Asn104	Asn146 & His148	H-bond
	Pro106	His148	VDW
β Framework	Leu74	Gln71 & Met72	VDW
	5-OP-RU	**TCR**	
	O4	Asp99β	H-bond

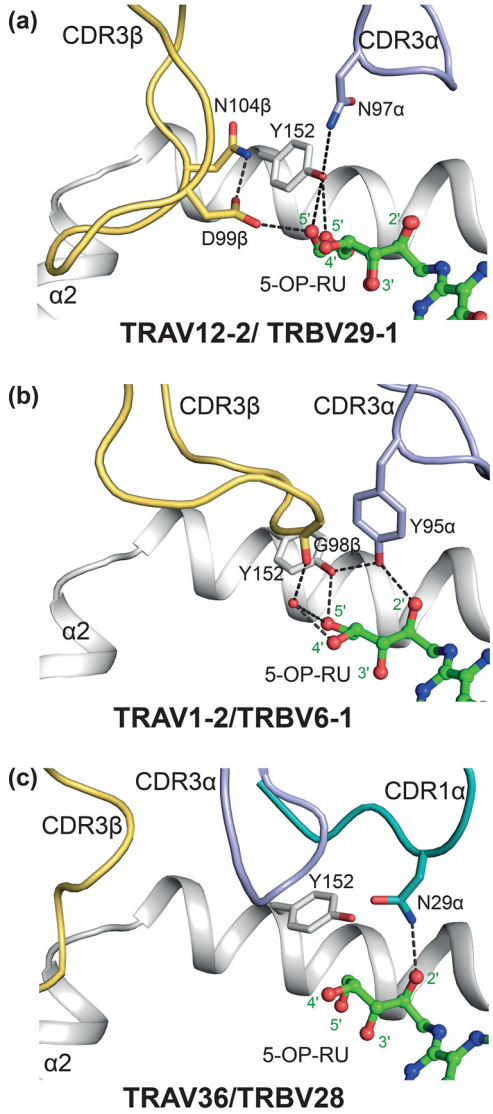

Figure 6. Recognition of riboflavin metabolite by TRAV1-2$^+$ and TRAV1-2$^-$ TCRs. *a*, interactions of the CDR3β of the D426-E4 TCR, depicting the direct and indirect polar contacts with 5-OP-RU ligand. *b*, interactions of CDR3α of TRAV1-2$^+$ A-F7 TCR with 5-OP-RU, showing the interaction triad between Tyr-152 of MR1, Tyr-95α of CDR3α, and 5-OP-RU. *c*, polar contacts of CDR1α of MAV36 TCR with 5-OP-RU, including the locations of CDR3α and CDR3β. The color coding is consistent with Figs. 3 and 5.

nonmicrobial ligands associated with MR1 (5, 15, 32). It is now established that the evolutionary conserved Tyr-95α from the CDR3α loop of TRAV1-2$^+$ TCRs forms an interaction triad with antigen 5-OP-RU and MR1 Tyr-152, and that this plays a prominent role in TRAV1-2$^+$ TCR recognition of the riboflavin-related antigens (2, 3, 6). For the CDR1α loop of the MAV36 TCR (TRAV36/TRAJ34), Asn-29α directly interacts with 5-OP-RU and MR1 Tyr-152 in a manner analogous to Tyr-95α (30). As such, the TRAV1-2$^+$ and MAV36$^+$ TCRs showed convergent mechanisms for recognition of riboflavin-related metabolites.

To examine how other TCRs might bind to MR1, we investigated here the recognition of a TRAV1-2$^-$ TCR (TRAV12-2–TRBV29-1). This D462-E4 TCR was able to recognize riboflavin-related as well as non–riboflavin-related MR1-bound ligands produced by *S. pyogenes* microbes (31), which suggested novel D462-E4 TCR docking and recognition strategies for metabolite antigens. Here, we found that this relatively rigid D462-E4 TCR docks centrally onto the MR1 antigen binding cleft but tilts toward and fully caps the F′ portal. Minor changes occurred for the TCR upon complexation with MR1. However, adaptable conformational changes within both the MR1-binding pocket and the 5-OP-RU ligand were observed upon TCR engagement.

Despite the usage of different TRAV genes, both TRAV12-2 of D462-E4 TCR and TRAV1-2 of A-F7 TCRs exhibit similar docking positions atop the A′-pocket of MR1, yet TRAV12-2 contributed much less to the MR1-binding interface (415 Å^2) compared with TRAV1-2 (580 Å^2). Further, none of the TRAV12-2 loops make contacts with the ligand. Indeed, the β-chain of TRBV29-01, in particular the CDR3β loop, plays a prominent role in D462-E4 recognition of the MR1-5-OP-RU complex. Here, the CDR3β loop extensively interacts with the empty F′-pocket of the MR1 antigen binding cleft. Moreover, Asp-99β from the CDR3β loop of the D462-E4 TCR interacted with the 5′-OH group of 5-OP-RU. As such our data demonstrate that the diverse MR1-reactive T cell repertoire exhibits varied docking strategies that enable divergent mechanisms to be used to recognize antigens bound to MR1.

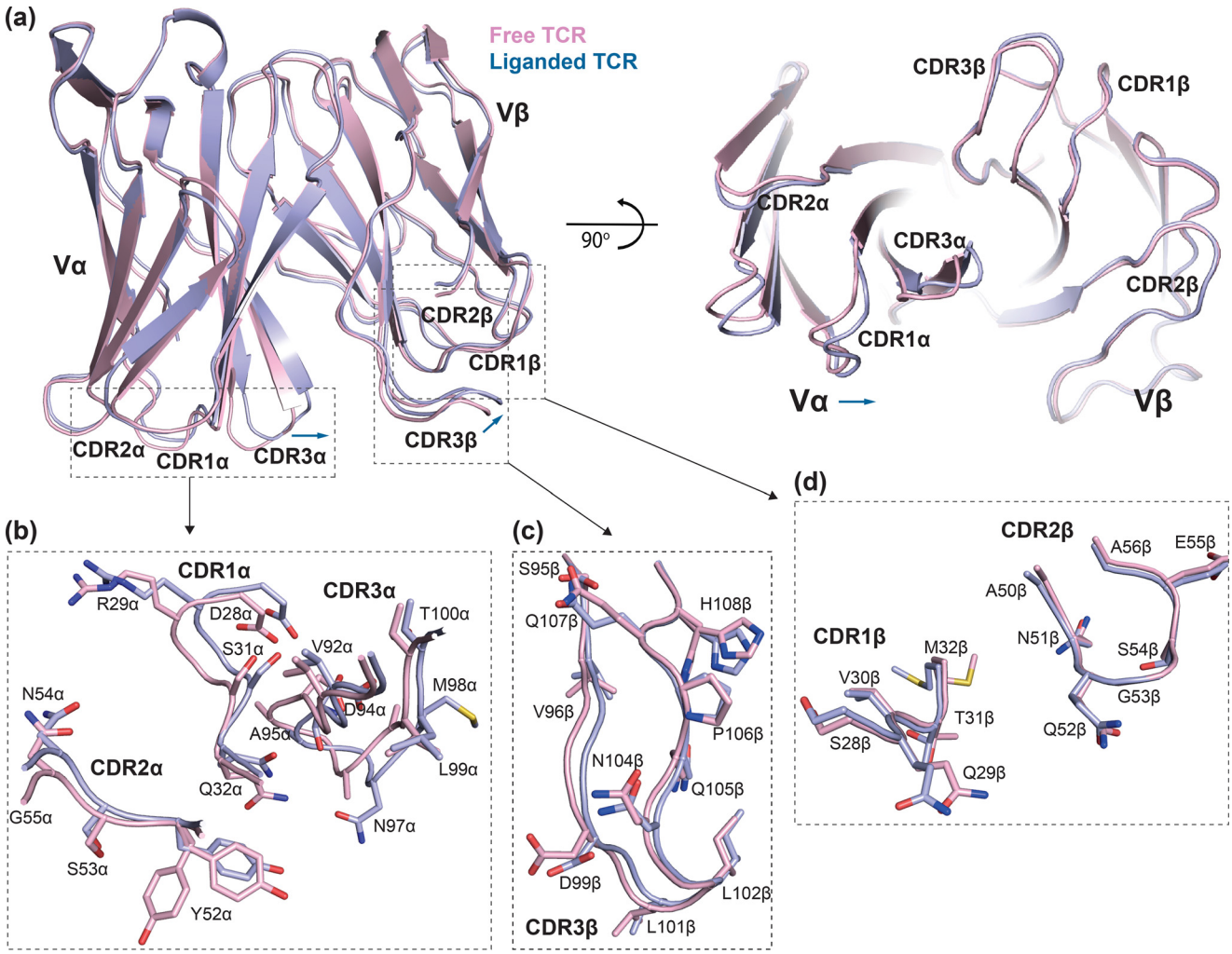

Figure 7. Comparison of free and liganded D426-E4 TCR structures. *a*, superposition of the variable domains (Vα and Vβ) of the free (*pink*) and bound to MR1 (*light-blue*) D426-E4 TCR. Vα and Vβ domains are shown as *ribbon*, and *arrows* show molecular adjustments of the variable domains upon complexation with MR1. The *right panel* shows the bottom view of various CDR loops. The TCRs were aligned via the variable domains of the two TCRs in PyMOL. *b*, the side chain residues of the CDR1α, CDR2α, and CDR3α loops of the aligned domains are shown as *sticks*. *c* and *d*, the side chain residues of CDR3β (*c*) and CDR1β and CDR2β (*d*) of the aligned structures are shown as *sticks*.

Experimental procedures

Cells and flow cytometry

MR1 restricted T cell clones were expanded using anti-CD3 and IL-2 and maintained as previously described (21, 31). Prior to sequencing TCRs, D462-E4 T cell clone was FACS purified after staining with LIVE/DEAD Fixable Dead Cell Stain Kit (Life Technologies) and an antibody for CD3. TRA and TRB TCR sequencing was performed by immunoSEQ (Adaptive Biotechnologies).

T cell clones were stained with MR1 tetramers (NIH Tetramer Core) for 1 h at room temperature. Cells were then washed with PBS + 2% FBS buffer and stained with LIVE/DEAD Fixable Dead Cell Stain Kit (Life Technologies) and surface stained with antibodies specific for CD3, CD4, CD8, and TRAV1-2 for 20 min at 4°C. Samples were fixed with 4% paraformaldehyde for 15 min and washed with a PBS + 2% FBS buffer, and acquisition was performed using a Fortessa flow cytometer with FACSDiva software (BD Biosciences). All flow cytometry data were analyzed using FlowJo software (Treestar) and Prism (GraphPad).

ELISPOT assays

For the plate-bound tetramer ELISPOT (tetraSPOT) assay, ELISPOT plates were coated with an anti–IFN-γ antibody, as described previously (Ref. 31). At the time of coating, MR1 tetramers (NIH Tetramer Core) were added to wells at concentrations between 0 and 5 nM per well. After overnight incubation at 4°C, ELISPOT plates were washed three times with sterile PBS and then blocked with RPMI 1640 + 10% human serum for 1 h. MAIT cell clones (2×10^4) were added to wells overnight. IFN-γ ELISPOTs were enumerated following development as described previously (Ref. 31). For the MR1-blocking tetraSPOT assays, MR1 blocking antibody (clone 26.5) or isotype control (mouse IgG2a) was added at 5 μg/ml in additional wells with the MR1–5-OP-RU tetramer.

Expression and preparation of denatured inclusion bodies of MR1 and TCRs proteins

Genes encoding soluble human MR1, β2m, TRAV1-2/TRAJ33, TRAV12-2/TRAJ39, TRBV6-1, and TRBV29-1

chains were expressed for 4 h in BL21 *E. coli* after induction with 1 mM isopropyl β-D-1-thiogalactopyranoside as described previously (1, 28). *E. coli* were pelleted and resuspended in a buffer containing 50 mM Tris-HCL, 10 mM DTT, 25% (w/v) sucrose, and 1 mM EDTA, pH 8.0. Then, the inclusion body protein was extracted by lysis of bacteria in a lysis buffer containing 50 mM Tris-HCL, pH 8.0, 10 mM DTT, 1% (w/v) Triton X-100, 1% (w/v) sodium deoxycholate, 100 mM NaCl, 5 mM $MgCl_2$ and 1 mg DNase I, and 2 mg lysozyme per liter of starting culture. Inclusion body protein was homogenized with a polytron homogenizer, then centrifugation and washing inclusion body protein sequentially, with 1) a buffer containing 50 mM Tris, pH 8.0, 1 mM DTT, 0.5% Triton X-100, 100 mM NaCl, and 1 mM EDTA and 2) a buffer containing 50 mM Tris, pH 8.0, 1 mM DTT, and 1 mM EDTA. Inclusion body was next resuspended in a buffer containing 20 mM Tris, pH 8.0, 1 mM DTT, 8 M urea, and 0.5 mM EDTA, and after centrifugation the supernatant containing solubilized, denatured inclusion body protein was collected and stored at −80°C.

Refolding and purification of MR1 and MR1-restricted TCRs

A-F7 (TRAV1-2/TRBV6-1) MAIT TCR and human MR1-β2m-6-FP, Ac-6-FP, and 5-OP-RU were refolded in the cold room overnight in the presence of 0.1 M Tris, pH 8.5, 5 M urea, 2 mM EDTA, 0.4 M L-arginine, 0.5 mM oxidized GSH, and 5 mM reduced GSH as described previously (1, 28). Similarly, D462-E4 (TRAV12-2/TRBV29-1) TCR was refolded at 4°C in 1 liter of refold buffer but with three injections of 50 mg of both α TRAV12-2 and β TRBV29-1 chains over 3 days. 5-OP-RU ligand was generated in situ in water from the addition of 5-A-RU and methylglyoxal as previously described (Ref. 2). Next, the refolded MR1-β2m-Ag and TCR proteins were then dialyzed against three changes of buffer containing 10 mM Tris-HCl, pH 8, over 24 h and purified by sequential crude DEAE anion exchange, size exclusion chromatography then HiTrap-Q HP anion exchange chromatography. The purity of the resulting protein was assessed using SDS-PAGE and further quantified by A280 absorbance.

Surface plasmon resonance measurements and analysis

All SPR experiments were conducted at 25°C, in duplicate (n = 3), on a BIAcore 3000 instrument using HBS buffer (10 mM HEPES-HCl, pH 7.4, 150 mM NaCl, and 0.005% surfactant P20) as described previously (28). Biotinylated MR1-β2m-Ag was immobilized on SA-Chip (GE Healthcare) with a surface density of ~2000 response units. Various concentrations (0–150 μM) of two MR1-restricted TCRs, A-F7 (TRAV1-2-TRBV6-1) and D462-E4 (TRAV12-2/TRBV29-1), were injected over the captured MR1-β2m-Ag at 5 μl/min and equilibrium data were collected. The final response was calculated by subtracting the response of the blank flow cell alone from the TCR-MR1-β2m-Ag complex. The SPR sensorgrams, equilibrium curves, and steady state K_D values (μM) were prepared using GraphPad Prism 7.

Crystallization, structure determination and refinement

Purified D462-E4 TCR was mixed with MR1-5-OP-RU in a 1:1 molar ratio at a concentration of 8–10 mg/ml and kept on ice for 2 h. Crystals of D462-E4 TCR-MR1-5-OP-RU ternary complex were grown by hanging-drop vapor diffusion method at 20°C, with a reservoir solution containing 18–26% PEG3350, 100 mM Bis-Tris Propane (pH 8.0–8.6) and 200 mM sodium bromide. Similarly, the binary D462-E4 TCR crystals were obtained at concentration of 5 mg/ml with a precipitant consisting of 16–24% PEG3350, 100 mM Bis-Tris Propane (pH 6.0–6.6), and 200 mM sodium fluoride. Both binary and ternary complexes crystals grew within 5–10 days, and then were flashed frozen in liquid nitrogen after quick soaking in reservoir solution with 10–12% glycerol for cryo-protection. X-ray diffraction data were collected at 100 K on the Australian Synchrotron at MX2 beamline (34). Diffraction images were processed using XDS (35) and programs from the CCP4 suite (36) and Phenix package (37). The D462-E4 TCR crystal structure was determined by molecular replacement using PHASER program (38) using an A-F7 TCR as search model (PDB ID: 4L4T). Next, we used the solved binary D462-E4 TCR and MR1 coordinates (PDB ID: 4L4T) as search model to solve the ternary structure of D462-E4 TCR-MR1-5-OP-RU complex. Manual model building was conducted using COOT (39), followed by iterative rounds of refinement using Phenix.refine (37). The Grade Webserver and Phenix tools were used to build and to generate ligand restraints. The models were validated using MolProbity (40) and the final refinement statistics are summarized in Table 2. All molecular graphic representations were generated using PyMOL Molecular Graphics System, Version 1.8, (Schrödinger, LLC, New York, NY). The buried surface area is calculated using AreaIMol program, the contacts generated by the Contact program, both from the CCP4 suite (36).

Data availability

The coordinates of the D462-E4 TCR and D462-E4 TCR-MR1–5-OP-RU crystal structures have been deposited in the Protein Data Bank under accession codes 6XQQ and 6XQP, respectively.

Acknowledgments—We thank the staff at the Monash Macromolecular Crystallization Facility for expert assistance. This research was undertaken in part using the MX2 beamline at the Australian Synchrotron, part of ANSTO, and made use of the Australian Cancer Research Foundation (ACRF) detector. We appreciate the assistance of Komagal Kannan Sivaraman.

Author contributions—W. A., E. W. M., J. L. N., and D. M. L. formal analysis; W. A. and J. L. N. investigation; W. A. and J. R. writing-original draft; W. A., D. P. F., D. M. L., and J. R. writing-review and editing; M. L. S.-R. methodology; J. L. N. and D. M. L. project administration; A. H. W. and M. D. N. data curation; L. L., D. P. F., J. M., and J. R. resources; J. M., D. P. F., D. M. L., and J. R. funding acquisition; D. M. L. and J. R. conceptualization; J. R. supervision.

Funding and additional information—This work was supported by Australian National Health and Medical Research Council (NHMRC) Grants 1125493 and 1113293 and Australian Research Council (ARC) Grant CE140100011. D. P. F. is an NHMRC Senior Principal Research Fellow (1117017), J. L. N. is an ARC Future Fellow (FT160100074), J.R. is an Australian ARC Laureate Fellow.

Conflict of interest—J. R., J. M., L. L., and D. P. F. are named inventors on patent applications (PCT/AU2013/000742, WO2014005194) (PCT/AU2015/050148, WO2015149130) involving MR1 ligands for MR1-restricted MAIT cells owned by University of Queensland, Monash University, and University of Melbourne.

Abbreviations—The abbreviations used are: MAIT, mucosal associated invariant T; TCR, T cell receptor; CDR, complementarity-determining region; Ag, antigen; SPR, surface plasmon resonance; BSA, buried surface area; rmsd, root mean square deviation.

References

1. Kjer-Nielsen, L., Patel, O., Corbett, A. J., Le Nours, J., Meehan, B., Liu, L., Bhati, M., Chen, Z., Kostenko, L., Reantragoon, R., Williamson, N. A., Purcell, A. W., Dudek, N. L., McConville, M. J., O'Hair, R. A. J., *et al.* (2012) MR1 presents microbial vitamin B metabolites to MAIT cells. *Nature* **491,** 717–723 CrossRef Medline
2. Corbett, A. J., Eckle, S. B. G., Birkinshaw, R. W., Liu, L., Patel, O., Mahony, J., Chen, Z., Reantragoon, R., Meehan, B., Cao, H., Williamson, N. A., Strugnell, R. A., Van Sinderen, D., Mak, J. Y. W., Fairlie, D. P., *et al.* (2014) T-cell activation by transitory neo-antigens derived from distinct microbial pathways. *Nature* **509,** 361–365 CrossRef Medline
3. Eckle, S. B. G., Birkinshaw, R. W., Kostenko, L., Corbett, A. J., McWilliam, H. E. G., Reantragoon, R., Chen, Z., Gherardin, N. A., Beddoe, T., Liu, L., Patel, O., Meehan, B., Fairlie, D. P., Villadangos, J. A., Godfrey, D. I., *et al.* (2014) A molecular basis underpinning the T cell receptor heterogeneity of mucosal-associated invariant T cells. *J. Exp. Med.* **211,** 1585–1600 CrossRef Medline
4. Lars, K.-N., Corbett, A. J., Chen, Z., Liu, L., Mak, J. Y., Godfrey, D. I., Rossjohn, J., Fairlie, D. P., McCluskey, J., and Eckle, S. B. (2018) An overview on the identification of MAIT cell antigens. *Immunol. Cell Biol.* **96,** 573–587 CrossRef Medline
5. Harriff, M. J., McMurtrey, C., Froyd, C. A., Jin, H., Cansler, M., Null, M., Worley, A., Meermeier, E. W., Swarbrick, G., Nilsen, A., Lewinsohn, D. A., Hildebrand, W., Adams, E. J., and Lewinsohn, D. M. (2018) MR1 displays the microbial metabolome driving selective MR1-restricted T cell receptor usage. *Sci. Immunol.* **3,** eaao2556 CrossRef Medline
6. Awad, W., Ler, G. J. M., Xu, W., Keller, A. N., Mak, J. Y. W., Lim, X. Y., Liu, L., Eckle, S. B. G., Le Nours, J., McCluskey, J., Corbett, A. J., Fairlie, D. P., and Rossjohn, J. (2020) The molecular basis underpinning the potency and specificity of MAIT cell antigens. *Nat. Immunol.* **21,** 400–411 CrossRef Medline
7. Keller, A. N., Eckle, S. B. G., Xu, W., Liu, L., Hughes, V. A., Mak, J. Y. W., Meehan, B. S., Pediongco, T., Birkinshaw, R. W., Chen, Z., Wang, H., D'Souza, C., Kjer-Nielsen, L., Gherardin, N. A., Godfrey, D. I., *et al.* (2017) Drugs and drug-like molecules can modulate the function of mucosal-associated invariant T cells. *Nat. Immunol.* **18,** 402–411 CrossRef Medline
8. Crowther, M. D., Dolton, G., Legut, M., Caillaud, M. E., Lloyd, A., Attaf, M., Galloway, S. A. E., Rius, C., Farrell, C. P., Szomolay, B., Ager, A., Parker, A. L., Fuller, A., Donia, M., McCluskey, J., *et al.* (2020) Genome-wide CRISPR–Cas9 screening reveals ubiquitous T cell cancer targeting via the monomorphic MHC class I-related protein MR1. *Nat. Immunol.* **21,** 178–185 CrossRef Medline
9. McWilliam, H. E. G., Eckle, S. B. G., Theodossis, A., Liu, L., Chen, Z., Wubben, J. M., Fairlie, D. P., Strugnell, R. A., Mintern, J. D., McCluskey, J., Rossjohn, J., and Villadangos, J. A. (2016) The intracellular pathway for the presentation of vitamin B-related antigens by the antigen-presenting molecule MR1. *Nat. Immunol.* **17,** 531–537 CrossRef Medline
10. Salio, M., Awad, W., Veerapen, N., Gonzalez-Lopez, C., Kulicke, C., Waithe, D., Martens, A. W. J., Lewinsohn, D. M., Hobrath, J. V., Cox, L. R., Rossjohn, J., Besra, G. S., and Cerundolo, V. (2020) Ligand-dependent downregulation of MR1 cell surface expression. *Proc. Natl. Acad. Sci. U. S. A.* **117,** 10465–10475 CrossRef
11. Meermeier, E. W., Harriff, M. J., Karamooz, E., and Lewinsohn, D. M. (2018) MAIT cells and microbial immunity. *Immunol. Cell Biol.* **96,** 607–617 CrossRef Medline
12. Treiner, E., Duban, L., Bahram, S., Radosavljevic, M., Wanner, V., Tilloy, F., Affaticati, P., Gilfillan, S., and Lantz, O. (2003) Selection of evolutionarily conserved mucosal-associated invariant T cells by MR1. *Nature* **422,** 164–169 CrossRef Medline
13. Le Bourhis, L., Martin, E., Péguillet, I., Guihot, A., Froux, N., Coré, M., Lévy, E., Dusseaux, M., Meyssonnier, V., Premel, V., Ngo, C., Riteau, B., Duban, L., Robert, D., Rottman, M., *et al.* (2010) Antimicrobial activity of mucosal-associated invariant T cells. *Nat. Immunol.* **11,** 701–708 CrossRef Medline
14. Reantragoon, R., Corbett, A. J., Sakala, I. G., Gherardin, N. A., Furness, J. B., Chen, Z., Eckle, S. B. G., Uldrich, A. P., Birkinshaw, R. W., Patel, O., Kostenko, L., Meehan, B., Kedzierska, K., Liu, L., Fairlie, D. P., *et al.* (2013) Antigen-loaded MR1 tetramers define T cell receptor heterogeneity in mucosal-associated invariant T cells. *J. Exp. Med.* **210,** 2305–2320 CrossRef Medline
15. Gherardin, N. A., McCluskey, J., Rossjohn, J., and Godfrey, D. I. (2018) The diverse family of MR1-restricted T cells. *J. Immunol.* **201,** 2862–2871 CrossRef Medline
16. Koay, H.-F., Gherardin, N. A., Xu, C., Seneviratna, R., Zhao, Z., Chen, Z., Fairlie, D. P., McCluskey, J., Pellicci, D. G., Uldrich, A. P., and Godfrey, D. I. (2019) Diverse MR1-restricted T cells in mice and humans. *Nat. Commun.* **10,** 2243 CrossRef Medline
17. Le Nours, J., Gherardin, N. A., Ramarathinam, S. H., Awad, W., Wiede, F., Gully, B. S., Khandokar, Y., Praveena, T., Wubben, J. M., Sandow, J. J., Webb, A. I., von Borstel, A., Rice, M. T., Redmond, S. J., Seneviratna, R., *et al.* (2019) A class of γδ T cell receptors recognize the underside of the antigen-presenting molecule MR1. *Science* **366,** 1522–1527 CrossRef Medline
18. Gibbs, A., Leeansyah, E., Introini, A., Paquin-Proulx, D., Hasselrot, K., Andersson, E., Broliden, K., Sandberg, J. K., and Tjernlund, A. (2017) MAIT cells reside in the female genital mucosa and are biased towards IL-17 and IL-22 production in response to bacterial stimulation. *Mucosal Immunol.* **10,** 35–45 CrossRef Medline
19. Lepore, M., Kalinichenko, A., Kalinicenko, A., Colone, A., Paleja, B., Singhal, A., Tschumi, A., Lee, B., Poidinger, M., Zolezzi, F., Quagliata, L., Sander, P., Newell, E., Bertoletti, A., Terracciano, L., *et al.* (2014) Parallel T-cell cloning and deep sequencing of human MAIT cells reveal stable oligoclonal TCRβ repertoire. *Nat. Commun.* **5,** 3866 CrossRef Medline
20. Dias, J., Sobkowiak, M. J., Sandberg, J. K., and Leeansyah, E. (2016) Human MAIT-cell responses to *Escherichia coli*: Activation, cytokine production, proliferation, and cytotoxicity. *J. Leukocyte Biol.* **100,** 233–240 CrossRef Medline
21. Gold, M. C., Cerri, S., Smyk-Pearson, S., Cansler, M. E., Vogt, T. M., Delepine, J., Winata, E., Swarbrick, G. M., Chua, W.-J., Yu, Y. Y. L., Lantz, O., Cook, M. S., Null, M. D., Jacoby, D. B., Harriff, M. J., *et al.* (2010) Human mucosal associated invariant T cells detect bacterially infected cells. *PLoS Biol.* **8,** e1000407 CrossRef Medline
22. Porcelli, S., Yockey, C. E., Brenner, M. B., and Balk, S. P. (1993) Analysis of T cell antigen receptor (TCR) expression by human peripheral blood CD4-8- alpha/beta T cells demonstrates preferential use of several V beta genes and an invariant TCR alpha chain. *J. Exp. Med.* **178,** 1–16 CrossRef Medline
23. Tilloy, F., Treiner, E., Park, S.-H., Garcia, C., Lemonnier, F., de la Salle, H., Bendelac, A., Bonneville, M., and Lantz, O. (1999) An invariant T cell receptor α chain defines a novel TAP-independent major histocompatibility complex class Ib–restricted α/β T cell subpopulation in mammals. *J. Exp. Med.* **189,** 1907–1921 CrossRef Medline
24. Dusseaux, M., Martin, E., Serriari, N., Péguillet, I., Premel, V., Louis, D., Milder, M., Le Bourhis, L., Soudais, C., Treiner, E., and Lantz, O. (2011)

Human MAIT cells are xenobiotic-resistant, tissue-targeted, CD161^{hi} IL-17–secreting T cells. *Blood* **117,** 1250–1259 CrossRef Medline
25. Tang, X.-Z., Jo, J., Tan, A. T., Sandalova, E., Chia, A., Tan, K. C., Lee, K. H., Gehring, A. J., De Libero, G., and Bertoletti, A. (2013) IL-7 licenses activation of human liver intrasinusoidal mucosal-associated invariant T cells. *J. Immunol.* **190,** 3142–3152 CrossRef Medline
26. Gold, M. C., McLaren, J. E., Reistetter, J. A., Smyk-Pearson, S., Ladell, K., Swarbrick, G. M., Yu, Y. Y. L., Hansen, T. H., Lund, O., Nielsen, M., Gerritsen, B., Kesmir, C., Miles, J. J., Lewinsohn, D. A., Price, D. A., *et al.* (2014) MR1-restricted MAIT cells display ligand discrimination and pathogen selectivity through distinct T cell receptor usage. *J. Exp. Med.* **211,** 1601–1610 CrossRef Medline
27. Reantragoon, R., Kjer-Nielsen, L., Patel, O., Chen, Z., Illing, P. T., Bhati, M., Kostenko, L., Bharadwaj, M., Meehan, B., Hansen, T. H., Godfrey, D. I., Rossjohn, J., and McCluskey, J. (2012) Structural insight into MR1-mediated recognition of the mucosal associated invariant T cell receptor. *J. Exp. Med.* **209,** 761–774 CrossRef Medline
28. Patel, O., Kjer-Nielsen, L., Le Nours, J., Eckle, S. B. G., Birkinshaw, R., Beddoe, T., Corbett, A. J., Liu, L., Miles, J. J., Meehan, B., Reantragoon, R., Sandoval-Romero, M. L., Sullivan, L. C., Brooks, A. G., Chen, Z., *et al.* (2013) Recognition of vitamin B metabolites by mucosal-associated invariant T cells. *Nat. Commun.* **4,** 2142 CrossRef Medline
29. Awad, W., Le Nours, J., Kjer-Nielsen, L., McCluskey, J., and Rossjohn, J. (2018) Mucosal-associated invariant T cell receptor recognition of small molecules presented by MR1. *Immunol. Cell Biol.* **96,** 588–597 CrossRef Medline
30. Gherardin, N. A., Keller, A. N., Woolley, R. E., Le Nours, J., Ritchie, D. S., Neeson, P. J., Birkinshaw, R. W., Eckle, S. B., Waddington, J. N., Liu, L., Fairlie, D. P., Uldrich, A. P., Pellicci, D. G., McCluskey, J., Godfrey, D. I., *et al.* (2016) Diversity of T cells restricted by the MHC class I-related molecule MR1 facilitates differential antigen recognition. *Immunity* **44,** 32–45 CrossRef Medline
31. Meermeier, E. W., Laugel, B. F., Sewell, A. K., Corbett, A. J., Rossjohn, J., McCluskey, J., Harriff, M. J., Franks, T., Gold, M. C., and Lewinsohn, D. M. (2016) Human TRAV1-2-negative MR1-restricted T cells detect S. pyogenes and alternatives to MAIT riboflavin-based antigens. *Nat. Commun.* **7,** 12506 CrossRef Medline
32. Lepore, M., Kalinichenko, A., Calogero, S., Kumar, P., Paleja, B., Schmaler, M., Narang, V., Zolezzi, F., Poidinger, M., Mori, L., and De Libero, G. (2017) Functionally diverse human T cells recognize non-microbial antigens presented by MR1. *eLife* **6,** e24476 CrossRef Medline
33. Narayanan, G. A., McLaren, J. E., Meermeier, E. W., Ladell, K., Swarbrick, G. M., Price, D. A., Tran, J. G., Worley, A. H., Vogt, T., Wong, E. B., and Lewinsohn, D. M. (2020) The MAIT TCRβ chain contributes to discrimination of microbial ligand. *Immunol. Cell Biol.* CrossRef Medline
34. Aragão, D., Aishima, J., Cherukuvada, H., Clarken, R., Clift, M., Cowieson, N. P., Ericsson, D. J., Gee, C. L., Macedo, S., Mudie, N., Panjikar, S., Price, J. R., Riboldi-Tunnicliffe, A., Rostan, R., Williamson, R., *et al.* (2018) MX2: A high-flux undulator microfocus beamline serving both the chemical and macromolecular crystallography communities at the Australian Synchrotron. *J. Synchrotron Radiat.* **25,** 885–891 CrossRef Medline
35. Kabsch, W. (2010) Integration, scaling, space-group assignment and post-refinement. *Acta Crystallogr. D Biol. Crystallogr.* **66,** 133–144 CrossRef Medline
36. Winn, M. D., Ballard, C. C., Cowtan, K. D., Dodson, E. J., Emsley, P., Evans, P. R., Keegan, R. M., Krissinel, E. B., Leslie, A. G., McCoy, A., McNicholas, S. J., Murshudov, G. N., Pannu, N. S., Potterton, E. A., Powell, H. R., *et al.* (2011) Overview of the CCP4 suite and current developments. *Acta Crystallogr. D Biol. Crystallogr.* **67,** 235–242 CrossRef Medline
37. Adams, P. D., Afonine, P. V., Bunkóczi, G., Chen, V. B., Davis, I. W., Echols, N., Headd, J. J., Hung, L. W., Kapral, G. J., Grosse-Kunstleve, R. W., McCoy, A. J., Moriarty, N. W., Oeffner, R., Read, R. J., Richardson, D. C., *et al.* (2010) PHENIX: A comprehensive Python-based system for macromolecular structure solution. *Acta Crystallogr. D Biol. Crystallogr.* **66,** 213–221 CrossRef Medline
38. McCoy, A. J. (2007) Solving structures of protein complexes by molecular replacement with Phaser. *Acta Crystallogr. D Biol. Crystallogr.* **63,** 32–41 CrossRef Medline
39. Emsley, P., and Cowtan, K. (2004) Coot: Model-building tools for molecular graphics. *Acta Crystallogr. D Biol. Crystallogr.* **60,** 2126–2132 CrossRef Medline
40. Chen, V. B., Arendall, W. B., 3rd, Headd, J. J., Keedy, D. A., Immormino, R. M., Kapral, G. J., Murray, L. W., Richardson, J. S., and Richardson, D. C. (2010) MolProbity: All-atom structure validation for macromolecular crystallography. *Acta Crystallogr. D Biol. Crystallogr.* **66,** 12–21 CrossRef Medline